ECCOMAS Congress 2016
VII European Congress on Computational Methods in Applied Sciences and Engineering
M. Papadrakakis, V. Papadopoulos, G. Stefanou, V. Plevris (eds.)
Crete Island, Greece, 5–10 June 2016

LOW BOOM/LOW DRAG SMALL SIZE SUPERSONIC AIRCRAFT DESIGN

Atsushi Ueno[1], Yasushi Watanabe[1], Itham Salah El Din[2], Richard Grenon[2] and Gérald Carrier[2]

[1] Japan Aerospace Exploration Agency
6-13-1 Osawa, Mitaka, Tokyo, 181-0015, Japan.
e-mail: {aueno, wata}@chofu.jaxa.jp

[2] Office National d'Etudes et de Recherches Aérospatiales
8 rue des Vertugadins, FR-92190, Meudon, France.
{itham.Salah_el_din, richard.grenon, gerald.carrier}@onera.fr

Keywords: Supersonic, Low boom/low drag design, Engine integration, Multidisciplinary design optimization.

Abstract. *The French Aerospace Lab (ONERA) and Japan Aerospace Exploration Agency (JAXA) conducted a collaborative research on low-boom and low-drag design of small size supersonic aircraft including engine integration perspective. In this collaborative research, the validation of low-boom design tools, the optimization study on engine position considering aerodynamics, acoustic, and propulsion performances, and the low-boom design of propulsion-airframe integrated (PAI) configuration were performed. In this paper, obtained results are summarized and the low-boom design of PAI configuration is focused on, because the sonic boom loudness is raised by the engine integration. The applied low-boom design tool is based on the free-form deformation and the equivalent area with consideration of the change of lift distribution due to deformations. Results show that the sonic boom loudness of PAI configuration can be reduced to almost the same loudness of glider configuration without engine by the horizontal tail optimization.*

1 INTRODUCTION

Research activities to realize environmental-friendly supersonic aircrafts are conducted all over the world [1, 2]. The major environmental constraint is the sonic boom. Pressure waves caused by objects flying at supersonic speed are integrated with each other during the propagation to the ground and finally coalesce into two shock waves called N wave, causing loud noise on the ground. The Concorde was prohibited from flying supersonically overland due to the sonic boom. Currently, ICAO (International Civil Aviation Organization) is trying to establish regulations on the sonic boom loudness and to set the threshold to allow overland supersonic flight, which accelerates research activities to realize low-boom as well as low-drag performances [3, 5]. Other environmental constraints are originated from the engine. They are the airport noise and the emission such as NOx and CO2. Reducing these environmental burdens depends largely on the engine itself. For instance, large bypass ratio decreases the engine exhaust velocity at take-off and improves the specific fuel consumption, which results in reduction of airport noise and emission. On the other hand, large bypass ratio increases engine weight and drag caused by the nacelle, which has negative impact on the emission. In addition, shock waves caused by the propulsion system potentially affect the low-boom performance. Thus, the engine should be considered in terms of integration with airframe. Based on the above discussions, the low-boom and low-drag design including engine integration perspective is the key to realize environmental-friendly supersonic aircrafts.

Japan Aerospace Exploration Agency (JAXA) conducted the flight experiment to demonstrate the low-boom design using axisymmetric bodies [6], and recorded the low-boom signature that can be used as the validation data for low-boom design tools. The French Aerospace Lab (ONERA) has experience of low-boom design through HISAC project. In order to integrate their experiences, ONERA and JAXA conducted the collaborative research on the low-boom and low-drag design including engine integration perspective from 2011 to 2016. The reference aircraft and its specifications are shown in Fig. 1. In this paper, obtained results are summarized and the low-boom design of propulsion-airframe integrated configuration is focused on.

Specification	
Length	53 m
Weight	60 ~ 70 ton
Cruise Speed	1.6 Mach
Range	3500 nm
Payload	36 ~ 50 passengers

Figure 1: Small size supersonic transport.

2 OVERVIEW OF COLLABORATIVE RESEARCH

In the collaborative research, the glider geometry designed by JAXA is used as the reference glider (Fig. 2). Design conditions are Mach number of 1.6 and lift coefficient of 0.15. The sonic boom signature of this glider shows double shock waves at front and aft booms (Fig. 2), which contributes to the low-boom performance. Here, the reflection factor on the ground is 1.9. In this research, ONERA is mainly in charge of the low-boom design based on the equivalent area. JAXA is mainly in charge of the engine integration. Work packages (WP) are shown in Fig. 3. WP1 is ONERA's activity, and low-boom design tools are validated using the experimental data acquired in the D-SEND#1 flight test conducted by JAXA [6]. WP2 is

JAXA's activity, and the engine integration is examined in terms of aerodynamics, acoustic, and propulsion perspectives. WP3 is conducted collaboratively by ONERA and JAXA to perform the low-boom and low-drag design including engine integration. Results are summarized in the following sections.

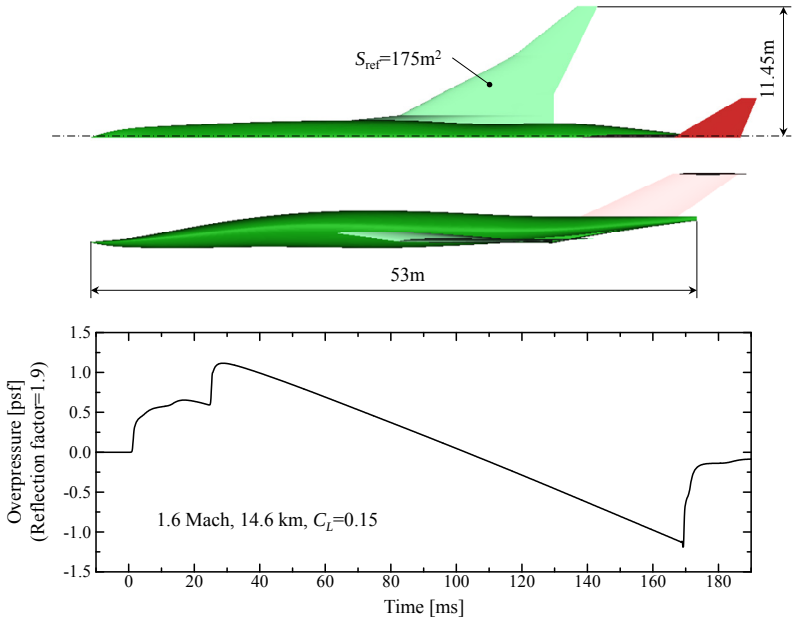

Figure 2: Reference glider and sonic boom signature.

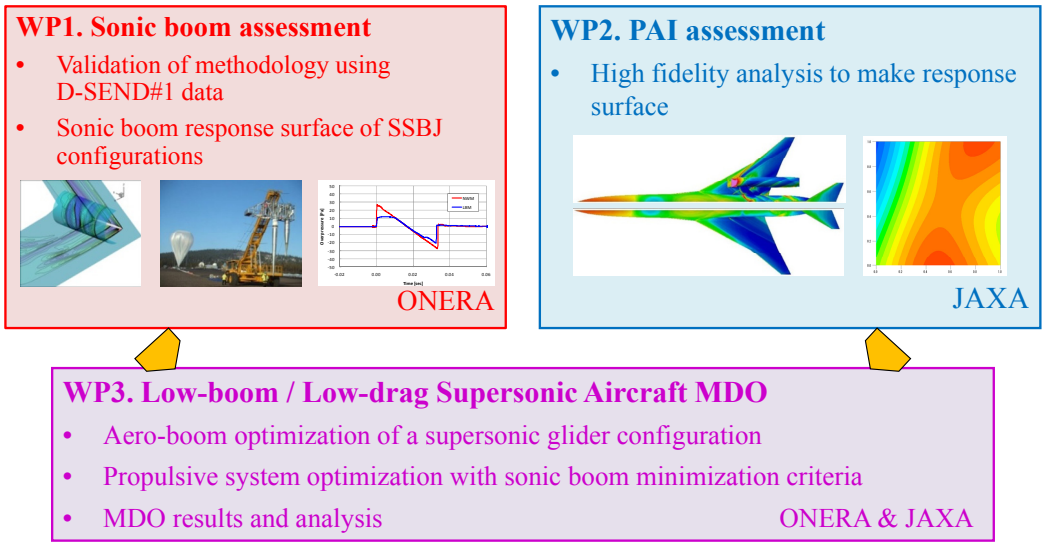

Figure 3: Work packages.

2.1 WP1: Sonic boom assessment

2.1.1. Sonic boom physics

Sonic boom signals are impulsive, high amplitude sound signals felt by a static observer at ground level. Sonic booms are the results of the nonlinear propagation through the atmosphere, down to the ground, of shock waves and pressure disturbances generated by supersonically travelling air vehicles such as aircraft, missiles or artillery projectiles [7]. The

displacement imposed by the supersonic vehicle to the air particles along its trajectory in its close vicinity are accompanied by pressure perturbations which radiate in all directions away from the vehicle along the three dimensional characteristics planes of the supersonic flow. A fraction of this pressure disturbances directed downward will eventually reach the ground after travelling through the atmosphere. During their propagation, the shape of the time signal associated to these pressure perturbations evolves under the competing non-linear and dissipative effects (Fig. 4). The non-linear effects tend to generate steep shocks through coalescence of successive pressure perturbations. On the contrary, the different dissipative effects, dominated by molecular relaxation phenomena, tend to thicken and dissipate shocks.

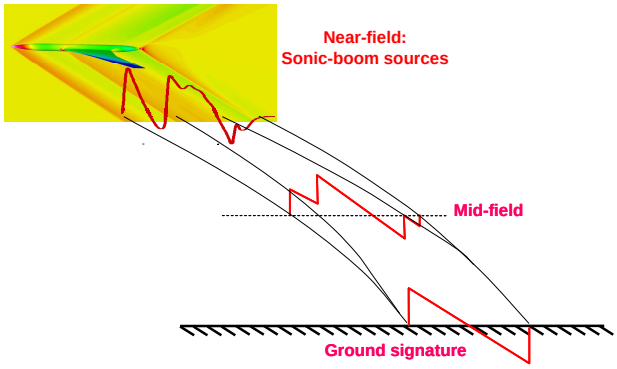

Figure 4: Sonic boom physics.

2.1.2. Methods and tools for calculating sonic boom

Simulating the sonic boom is an intricate task involving complex physical phenomena and very different scales. An accurate modeling of sonic boom first requires an adequate prediction of its sources, the aerodynamic pressure disturbances generated by the aircraft in its close vicinity. In this region, the aerodynamic flow is governed by the non-linear Euler equations and includes three-dimensional features with scales proportional to the aircraft length. Therefore CFD methods are perfectly suited and necessary to predict these near-field aerodynamic perturbations giving birth to the sonic boom. Because the prediction of the sonic boom requires propagating the pressure signal from the aircraft down to the ground over tens of kilometers, i.e. several hundreds of the aircraft length, conventional CFD methods are inadequate to perform this long distance propagation. They would require a tremendous number of mesh points and would eventually fail to capture important effect occurring during the propagation (such as the molecular relaxation). Therefore, a specific acoustic code is necessary to carry out this long distance propagation of the sonic boom signal through the standard atmosphere that is stratified and include temperature and density evolution with altitude.

The ONERA sonic boom prediction methodology is based on a three-layer approach, as illustrated in Fig. 5. Layer 1 corresponds to the near-field aerodynamic flow prediction with CFD. Layer 3 is the atmospheric propagation of the sonic boom with an acoustic code, while layer 2 ensures a natural matching between the near-field aerodynamic data and the native inputs of the acoustic code.

Layer 1: Near field aerodynamic calculation by CFD

First, the pressure perturbations in the close vicinity of the aircraft flying in supersonic cruise condition, which are the origin of the sonic boom, are calculated by solving the three-dimensional steady Euler equations. The ONERA *elsA* [8] or *Cedre* [9] CFD softwares are

used to perform these calculations. To obtain an accurate evaluation of the near-field aerodynamic pressure perturbations, a specific care must be given to the quality of the CFD mesh which must have characteristics adapted to the flow physics of these perturbations travelling along flow characteristics. The computational domain of this CFD calculation typically extends between twice and four times the aircraft length around the aircraft.

Layer 2: Multipole matching method

The CFD-aerodynamic pressure field is extracted on a cylinder surrounding the aircraft, aligned with the flow direction, whose radius is a user-specified parameter varying between one half to one body length. The pressure perturbations on this cylinder are then post-processed using the multipole decomposition method originally introduced by Plotkin and Page [11] and applied by Salah El Din [12]. This decomposition method proceeds through a development of the near field pressure signature on the cylinder according to the azimuth variable **θ.** Thereby, it allows to rebuild a Whitham function equivalent, at long distance, to the pressure perturbation generated by the aircraft, while cumulating the diffraction effects associated to the non-axisymmetrical near-field flow. The ground signature computed from this equivalent rebuilt Whitham function is observed to converge much faster with the matching distance between the CFD and the acoustic theory (i.e. the radius of the cylinder) than the ground signature from a direct CFD/acoustic would match. This justifies the use of this second layer which, further to provide a theoretically correct near-field/far-field match, greatly reduces the CFD grid size needed for the near field computation, saving significant computing time.

Layer 3: Atmospheric non-linear acoustic propagation method

Finally, the ground signature is computed by propagating the near-field aerodynamic pressure perturbations matched by the multipole decomposition method (layer 2) using the acoustic propagation code *TRAPS* [13]. The *TRAPS* code is a dedicated sonic boom propagation code based on the inviscid non-linear acoustic theory. It uses a ray-tracing approach to account for the refraction phenomena occurring during the propagation through a stratified atmosphere with vertical temperature and density gradients and to evaluate the extent of the "primary carpet", i.e. the width of the corridor underneath the aircraft trajectory directly affected by sonic boom. Along each acoustic ray, the Whitham theory (first order correction to the linear supersonic theory) is used to predict the evolution of the shape of the sonic boom pressure signal.

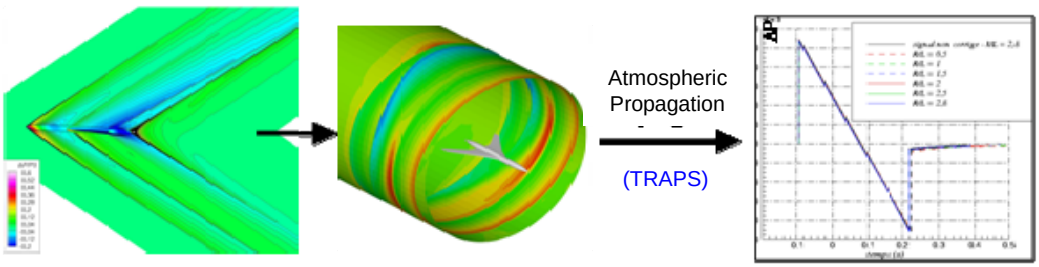

Figure 5: Three-layer sonic-boom prediction methodology.

2.1.3. Validation of the numerical sonic boom prediction tools

The sonic boom prediction tools used by ONERA have been validated using the JAXA D-SEND#1 experimental data [14]. These experiments consisted in a vertically drop test of two different models from a balloon high altitude: an N-Wave Model (NWM) and a Low-Boom Model (LBM) were tested (Fig. 6). During these drop tests, sonic booms have been measured at different locations including two microphones, one at ground level and the second at about 1km altitude, just above atmospherically turbulent boundary layer (Fig. 7).

The exact "flight" conditions of the model during its drop at the time when it generated the registered sonic boom signal on ground were determined through an analysis of the trajectory data using an inverse ray-tracing procedure. The near field aerodynamic signatures generated by both models in the previously identified flight conditions (Mach, altitude) were then computed using CFD calculations performed with the [9] software and mesh adaptations performed with INRIA mesh adaptation tool FEFLOA [10]. The sonic boom has then been computed at ground level using the methods and tools described in the previous section and the results compared to the D-SEND#1 tests data (Fig. 8).

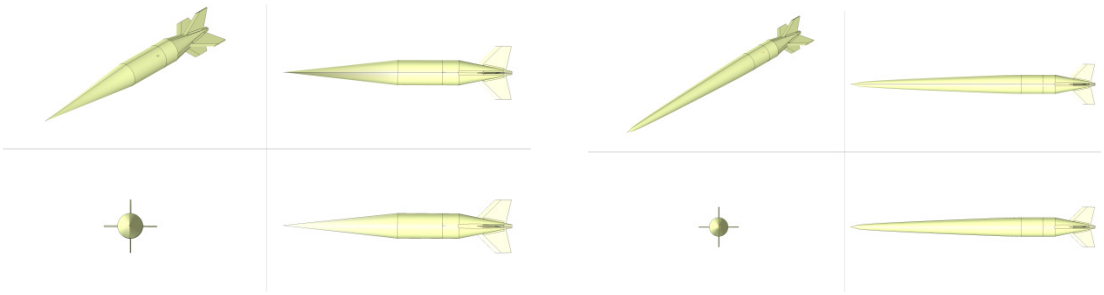

Figure 6: D-SEND#1 models geometry: conventional N-wave signature model (left) and low-boom flat top model (right).

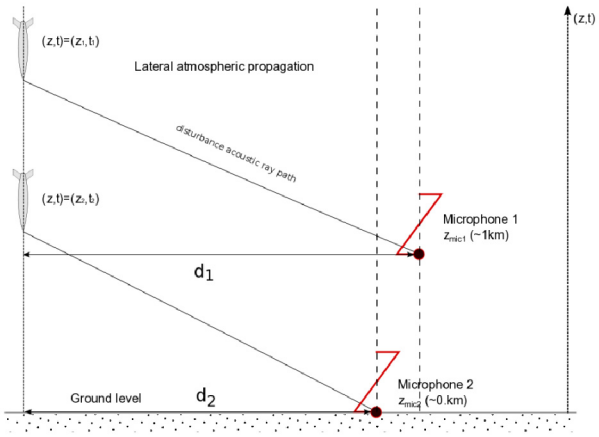

Figure 7: Schematic of JAXA D-SEND#1 drop tests sonic boom propagation: vertical descending trajectory of the model and oblique acoustic ray pointing downward; Position of the two microphones measuring the sonic boom at ground level and immediately above turbulent atmospheric boundary layer.

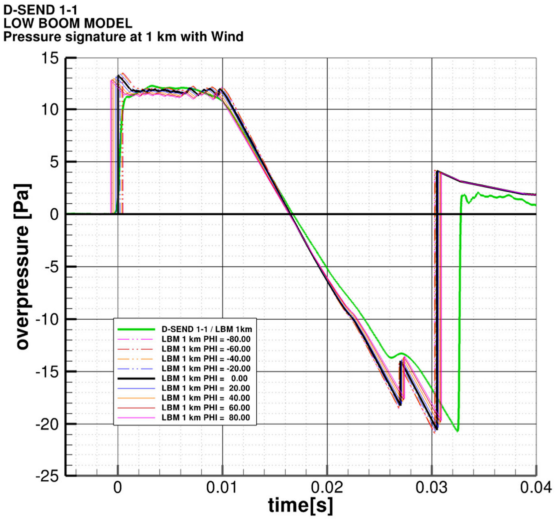

Figure 8: Validation of numerical sonic boom prediction tools using the JAXA D-SEND#1 experimental test results for the Low-boom model.

2.2 WP2: PAI assessment

In WP2, the engine integration is examined in terms of low-boom and low-drag [15, 16]. Supersonic engines generally tend to have smaller bypass ratio than subsonic engines, and increase airport noise. In this study, the engine specification was optimized to maximize the range performance while the engine exhaust velocity is constrained to be less than the specified value that can satisfy ICAO regulation (chapter 4). As a result, the bypass ratio and the fan diameter become 3.4 and 1.7 m, respectively. The inlet/nacelle geometry is designed based on the optimized engine specification and is integrated with the reference glider shown in Fig. 2. The design space of engine position is determined in this integration (Fig. 9), and response surfaces of lift-to-drag ratio and sonic boom loudness are constructed by the Euler analysis. Moreover, the engine position affects the propulsion performance such as inlet pressure recovery, thrust, and specific fuel consumption, which in turn affects the range performance. Thus, the inlet pressure recovery evaluated by the Navier-Stokes analysis is added to objective functions of response surfaces. These three objective functions are evaluated at the design lift coefficient (0.15). Response surfaces of side-body engines are shown in Fig. 10 as a typical example. There are 9 samples denoted by 01 ~ 09 in Fig. 10. Response surfaces are initially constructed by samples 01 ~ 08. Sample 09 is added considering the convergence of nondominated front in the optimization of engine position performed in WP3. Each axis in Fig. 10 is non-dimensionalized by the range of design space, that is, 0 corresponds to x_{min} and z_{min}, and 1 corresponds to x_{max} and z_{max}. The sonic boom loudness is evaluated in terms of the Stevens Perceived Level Mark VII (PL), and the difference of PL from that of the reference glider (97.1 dB) is the objective function. The inlet pressure recovery is the ratio of total pressure at engine fan face to total pressure of uniform flow. According to Fig. 10, the position of maximum lift-to-drag ratio and the position of minimum sonic boom loudness come close to each other, thus, the side-body engine can realize good compromise between low-boom and low-drag. On the other hand, the inlet pressure recovery is low at the position of maximum lift-to-drag ratio, which indicates the necessity of further investigation considering the propulsion performance. Therefore, the optimization in terms of low-boom and range performance including propulsion performance is conducted and is described in WP3.

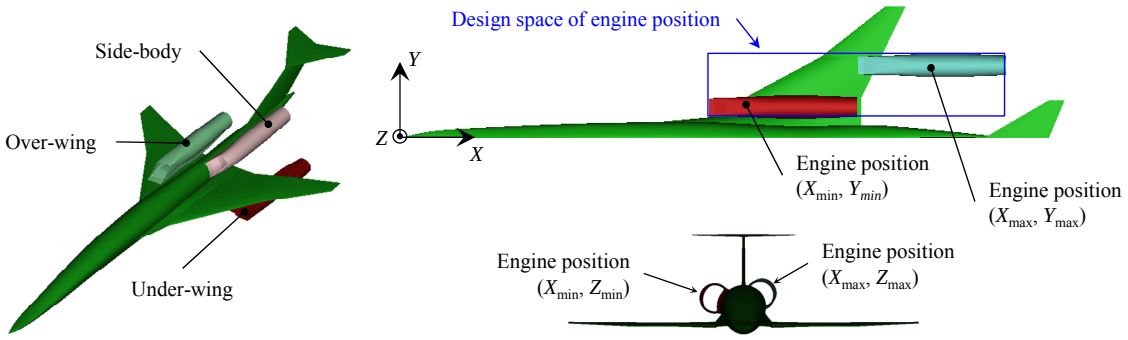

Figure 9: Design space of engine position.

Over- and under-wing		Side-body	
X_{min}	28.514 m	X_{min}	28.514 m
X_{max}	41.508 m	X_{max}	41.508 m
Y_{min}	2.756 m	Z_{min}	1.908 m
Y_{max}	6.306 m	Z_{max}	2.332 m

Table 1: Design space of engine position.

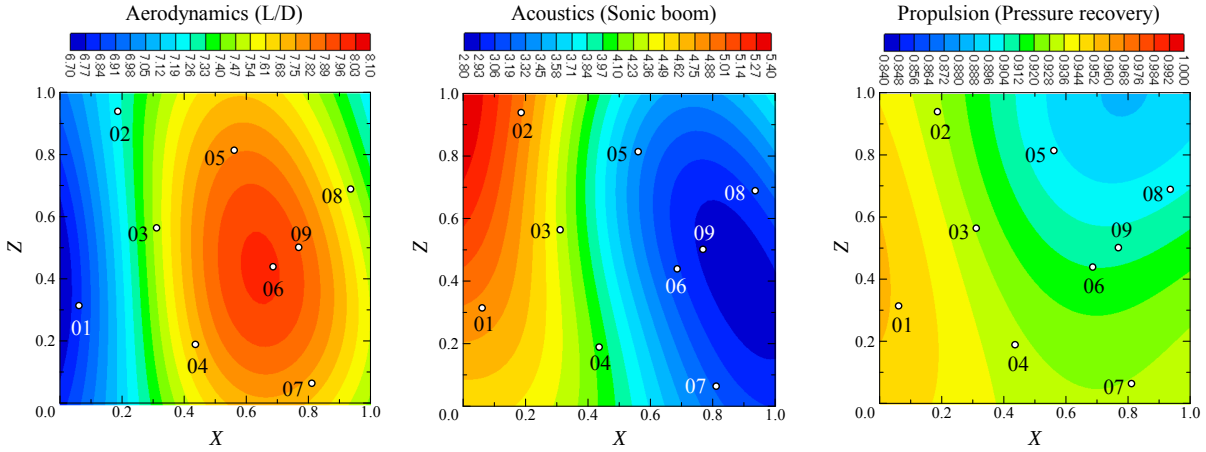

Figure 10: Response surfaces of side-body engine.

2.3 WP3: Low-boom/Low-drag Supersonic Aircraft MDO

Work package 3 includes the low-boom design of the reference glider that was conducted by ONERA and the optimization of engine position using response surfaces in WP2 that was conducted by JAXA. The low-boom design of engine-airframe integrated configuration based on results obtained here is described in the next chapter.

Aero-boom optimization of a supersonic glider configuration

A sonic boom minimization process of the initial wing-body-tail (glider) configuration has been performed by ONERA. This has been done using a two-step approach:

1. First, an inverse design approach, AIDA [4], implementing the Jones-Seebass-Darden shaped sonic boom theory, has been used to generate the minimum sonic

boom equivalent area ruling corresponding to the JAXA small supersonic aircraft characteristics (Mach number, fuselage length, weight, wing position, …);

2. Then, starting from the actual geometry of the initial glider configuration, a free-form deformation approach has been used to modify the actual fuselage geometry in order to reach the target equivalent area distribution issued from step 1). This was done through a numerical optimization process that used the vertical displacement of the different control points of the free-form lattice embedding the fuselage geometry as design parameter (Fig. 11). In this optimization process, only the impact of the geometry modifications on the equivalent area distribution due to volume was evaluated (the contribution of lift to the equivalent area was assumed to be constant).

The results of this design process applied to the glider configuration are shown in Fig. 12. The front part of the equivalent area was successfully mapped to the target one obtained by inverse design with AIDA module [4]. This enables to obtain a ground sonic boom whose front part resembles the target flat top signal even if it includes a succession of small shocks. The aft part of the signature was not significantly modified due to a limited design freedom (the control box was defined in order to keep the tail geometry unchanged).

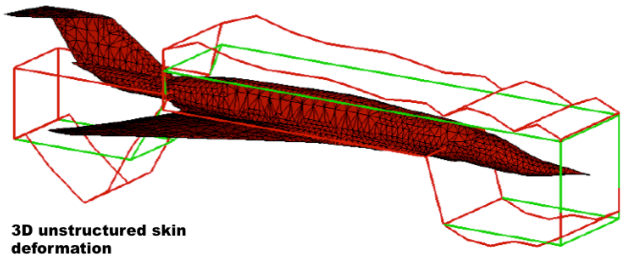

Figure 11: Free-form deformation control lattice used to optimize the fuselage geometry in order to reach the target equivalent area distribution that provides optimal sonic boom signature.

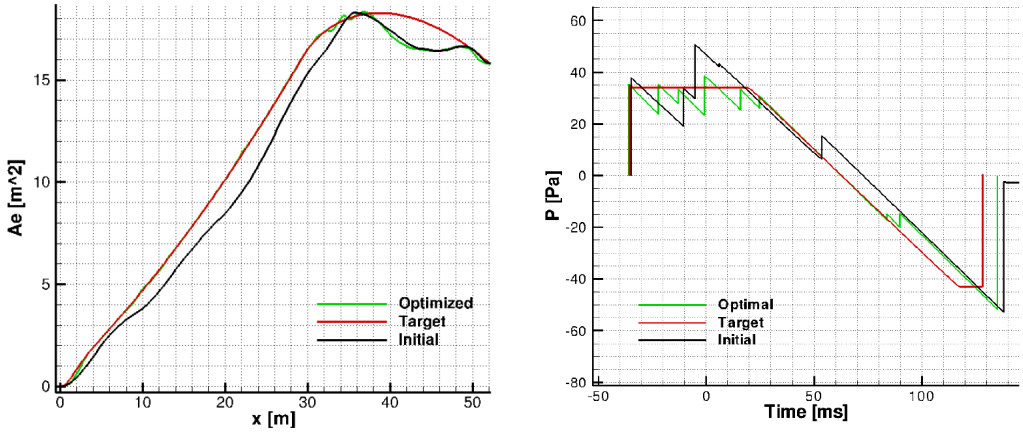

Figure 12: Left: initial, optimized and target equivalent area distribution. Right: ground propagated sonic boom signals corresponding to the initial glider, optimized glider and target optimal (flat-top) sonic boom.

Latter, such a similar design procedure using a free-form deformation parameterization and a target equivalent area distribution was reapplied to the complete aircraft geometry including propulsion system (Fig. 13).

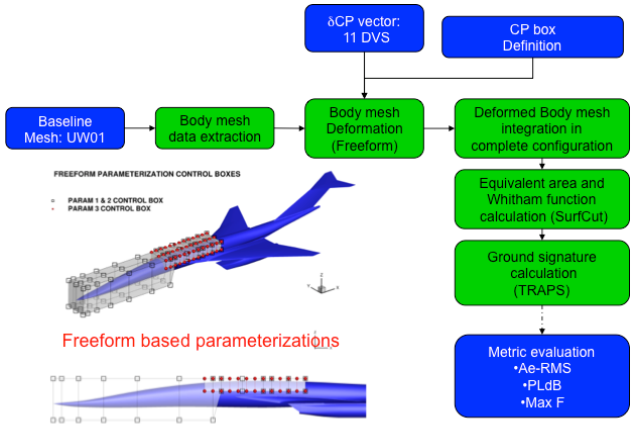

Figure 13: Application of a free form deformation based optimization process to reduce the sonic boom of the aircraft configuration with propulsion system.

Propulsive system optimization with sonic boom minimization criteria

The optimization of engine position is based on the response surfaces obtained in WP2 (Fig. 10) [16], which means that the glider geometry is fixed at the reference glider geometry and that the glider optimization tool mentioned above is not applied. In this optimization, two objective functions are set. One is the sonic boom loudness that is obtained directly from the response surface. The other is the range performance that is evaluated by the Breguet range equation using the lift-to-drag ratio and the specific fuel consumption that includes the performance degradation caused by the inlet pressure recovery. The nondominated front is shown in Fig. 14.

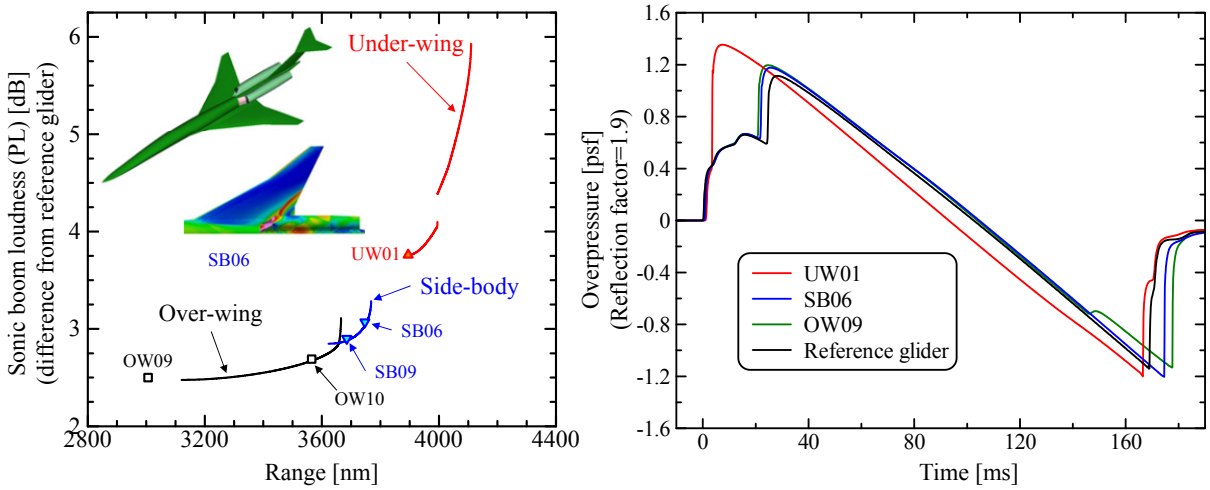

(a) Nondominated front with respect to sonic boom and range. (b) Sonic boom signature.

Figure 14: Optimization of engine position.

The under-wing engines realize large lift-to-drag ratio thanks to the compression lift produced by the nacelle shock wave, and realize large inlet pressure recovery because the stream line under the wing is nearly parallel to the inlet axis. Thus, the under-wing engines realize better range performance. However, the nacelle shock wave propagates to the ground and causes louder sonic boom. The over-wing engines show the best low-boom performance by shielding the nacelle shock wave by the wing upper surface, but the cross-flow over the wing degrades the inlet pressure recovery. Smaller lift-to-drag ratio due to the negative lift caused by the na-

celle shock wave along with low inlet pressure recovery leads to low range performance. The side-body engines overcome drawbacks mentioned above. The nacelle shock wave acts around the trailing edge of the wing, which reduces the wing pressure drag and prevents the nacelle shock wave from propagating to the ground. Thus, the low-boom and low-drag are realized at the same time. The inlet pressure recovery is relatively low due to the thick boundary layer on the fuselage; however, the side-body engines show better compromise between low-boom and long-range.

Results mentioned above are integrated, in other words, the glider optimization tool is applied to the side-body engine in order to realize further low-boom performance. The optimization results are described in the next section.

3 AFT BOOM SUPPRESSION BY HORIZONTAL TAIL OPTIMIZATION

Prior to the low-boom design, the sample 06 of side-body engine denoted by SB06 (Fig. 14) is slightly modified in order to reduce the wave drag. The engine position of modified SB06 denoted by PAI (propulsion-airframe integrated) configuration is almost the same as that of SB06, moved rearward and upward by 0.5% and 0.2% of fuselage length, respectively. The engine nozzle of SB06 is tangential to the fuselage at its exit. On the other hand, the part of engine nozzle (7% of the nozzle exit diameter) of PAI configuration is buried into the fuselage, and the wave drag is reduced due to the reduction of fuselage volume. The PAI configuration has larger lift-to-drag ratio by 3.2% than SB06. The PAI configuration and SB06 show almost the same sonic boom signature (Fig. 14), causing louder sonic boom than the reference glider due to the single shock wave at the aft boom. The engine nacelle produces negative lift, and the angle of attack is increased to meet design lift coefficient. As a result, the expansion over the wing is enhanced and the peak negative pressure at the aft boom is increased. Another reason to the louder aft boom is the expansion wave at the rear part of the nacelle. The shock wave at the leading edge of the horizontal tail plays an important role in fragmenting the aft boom into double shock waves. In the PAI configuration, the leading edge shock wave is weakened by the expansion wave originated from the nacelle (Fig. 15), and pressure waves coalesce into single shock wave at the aft boom. As shown in Fig. 14, over-wing engines realizing quieter sonic boom than side-body engines also show the single shock wave at the aft boom. These results indicate the importance of the aft boom suppression of propulsion-airframe integrated configurations. Thus, the low-boom design of the PAI configuration is conducted by applying the glider optimization tool described in WP3.

Equivalent area distributions of reference glider and PAI configuration are shown in Fig. 16. Both configurations have the peak value of equivalent area at x of around 60 m. This peak is made up by the shock wave and expansion wave of the horizontal tail. The aft boom of the reference glider is fragmented into double shock waves by the shock and expansion waves corresponding to the front and rear parts of the peak, respectively. This fragmentation is the key to reduce the aft boom loudness. In the PAI configuration, the shock wave is weakened by the expansion wave generated at the rear part of the nacelle as described above, which lowers the peak and degrades low-boom performance. To suppress the aft boom of the PAI configuration, the target equivalent area distribution with higher peak is determined (Fig. 16), and the profile of the horizontal tail that is originally the biconvex is optimized by free-form deformation (FFD) to meet the target.

In this optimization study, the low-boom design tool applied in WP3 is updated to consider the change of lift distribution, because the horizontal tail has impact on the lift. In this update, the change of lift caused by the deformation of horizontal tail is evaluated by the simple method, that is, the conical flow theory and the Prandtl-Meyer expansion. Firstly, the horizon-

tal tail surface is divided into triangle panels, and the angle between the panel and uniform flow is calculated for each panel. When the panel is facing the uniform flow, the pressure coefficient is evaluated by the conical flow theory. Otherwise, the pressure coefficient is evaluated by the Prandtl-Meyer expansion. After the deformation, the pressure coefficient is evaluated in the same manner, and the difference of the pressure coefficient due to the deformation gives the change of lift. The flow diagram of the updated tool is shown in Fig. 17. The horizontal tail is deformed by FFD and the volume component of equivalent area (AE_vol) is calculated. Then, the difference of the pressure coefficient is evaluated and the lift component of equivalent area (AE_lift) is calculated. The sum of AE_vol and AE_lift gives the equivalent area (AE), and FFD is iterated until the AE meets the target equivalent area (AE_target). After the iteration, the Euler analysis is conducted for the optimized shape to evaluate the low-boom performance.

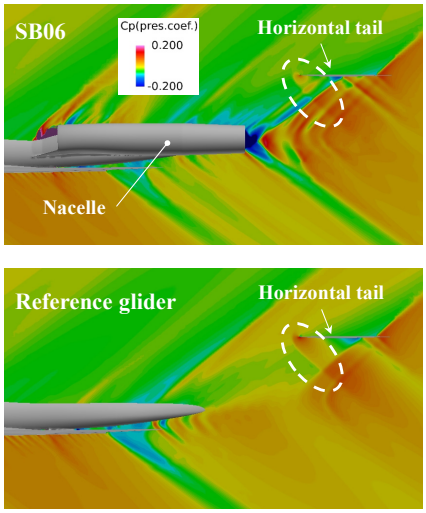

Figure 15: Pressure contour plot around nacelle.

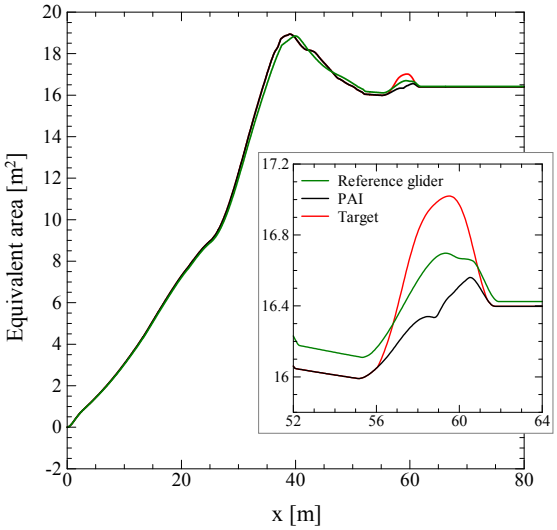

Figure 16: Equivalent area distribution.

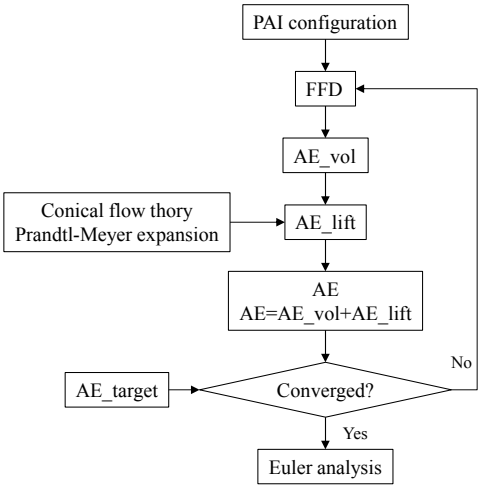

Figure 17: Flow diagram of horizontal tail optimization.

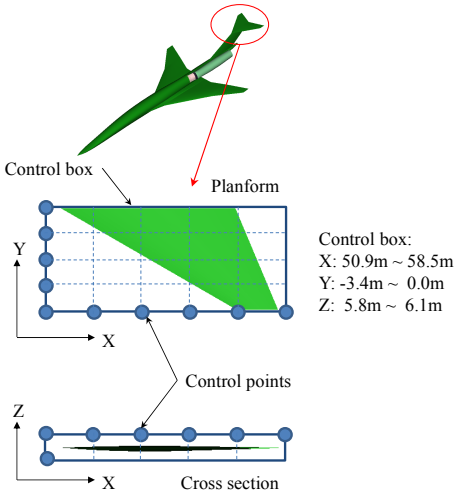

Figure 18: Free form deformation.

In FFD optimization, the rectangular parallelepiped control box is set to enclose the horizontal tail (Fig. 18). Numbers of control points are 6 in the *x* direction, 5 in the *y* direction, and 2 in the *z* direction. Design variables are the displacement of control points in the *z* direc-

tion, except for the control points on the symmetric surface (i.e., y=0). In order to check the convergence, the difference of equivalent area from the target is calculated at 81 sections between x of 56.0475 m and 61.3475 m where the equivalent area is affected by the horizontal tail deformation. The root mean square of these differences is the objective function (F). In this optimization, the drag increment due to the deformation is added to the objective function in order to realize both low-boom and low-drag (Eq. 1).

$$F = \left(\frac{1}{N} \sum_{i=1}^{N} \left(\mathrm{AE}_i - \mathrm{AE\_target}_i \right)^2 \right)^{0.5} + 10 \cdot \Delta C_D \tag{1}$$

Here, N is the number of sections where the difference of equivalent area from the target is calculated and is 81 as described above. The objective function is minimized by the optimizer based on the genetic algorithm. The constraint function is not defined, however, the lift coefficient is implicitly constrained to be unchanged, because AE_target has the same equivalent area at the tail end (at x=63 m) as the PAI configuration.

As a result of the optimization, the root tail-section has larger thickness to chord ratio and larger incidence angle (Fig. 19), causing larger lift and stronger shock wave. At the tip section, the incidence angle becomes smaller to cancel the lift increment at the root section, because lift coefficient is implicitly fixed at design C_L (0.15). The Euler analysis of the optimized shape shows that the lift coefficient of horizontal tail is changed by only 0.2%, which demonstrates the effectiveness of simplified method in the evaluation of lift change. Thanks to these changes of horizontal tail profile, the peak value of equivalent area is raised to meet the target (Fig. 20), and the aft boom is successfully fragmented into double shock waves (Fig. 21). The aft boom loudness, which is evaluated using the pressure signature where the pressure is negative, is reduced by 4.5 dB. The overall loudness is reduced by 2.9 dB. On the other hand, the drag is increased by 3 drag count mainly due to the thicker profile at the root section, though the smaller incident angle at the tip section contributes to the drag reduction. The nondominated front with respect to lift-to-drag ratio and sonic boom loudness obtained in WP3 is shown in Fig. 22. In this figure, the PAI configuration and the optimized shape are added. The reduction of lift-to-drag ratio is 1.8%. Though the optimization without the drag increment in the objective function (Eq. 1) is not performed, the nondominated front with respect to low-boom and low-drag is expected to be obtained by changing the scale factor of drag increment (10 in this study). As for the sonic boom loudness, it is largely reduced to almost the same level of the reference glider, which indicates the effectiveness of the low-boom design tool.

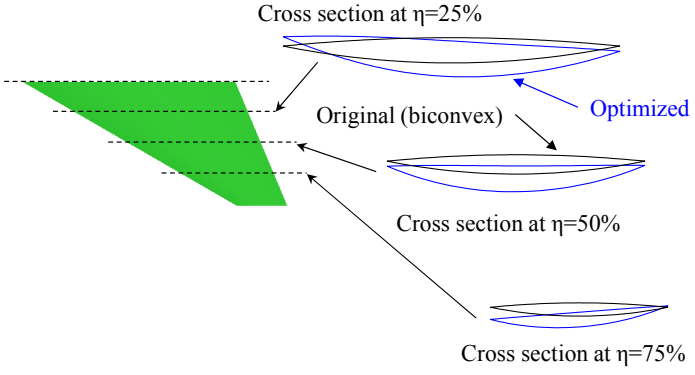

Figure 19: Optimized profile of horizontal tail.

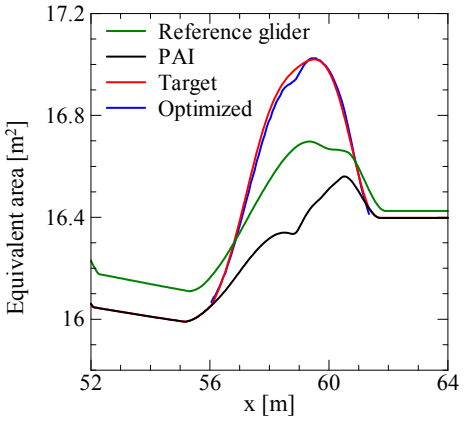

Figure 20: Optimized equivalent area distribution.

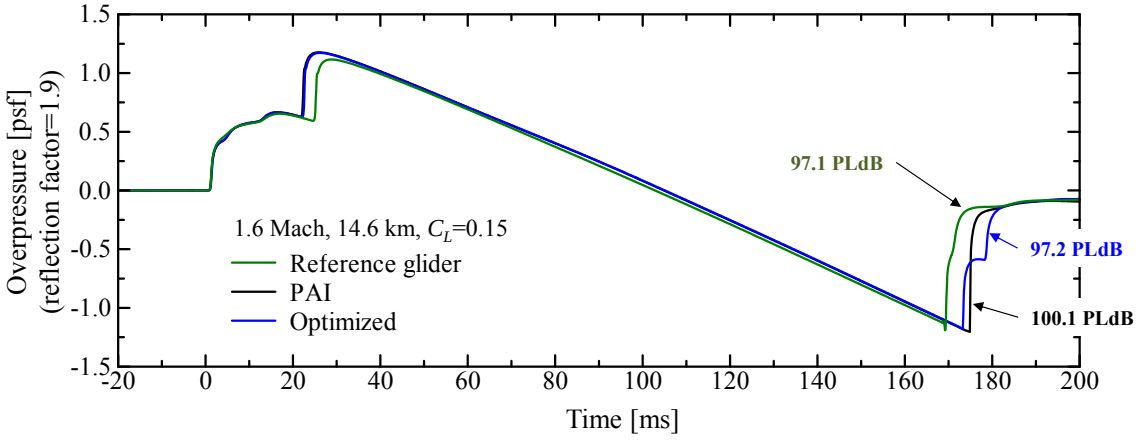

Figure 21: Optimized sonic boom signature.

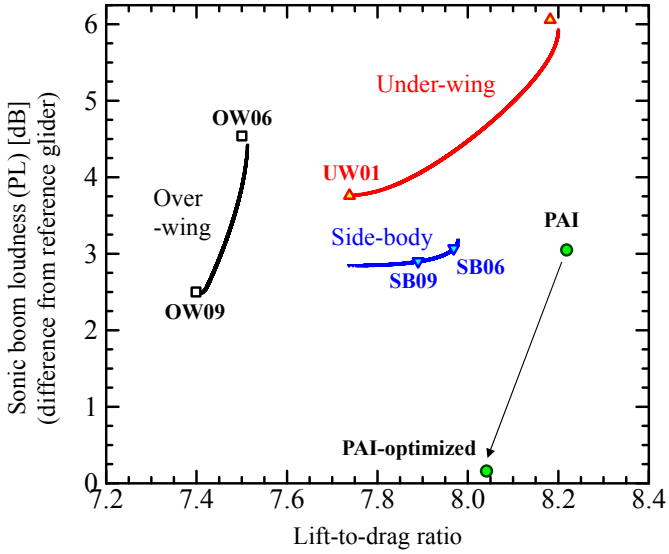

Figure 22: Nondominated front with respect to sonic boom and lift-to-drag ratio.

4 CONCLUSION

The low-boom and low-drag design of small size supersonic aircraft including engine integration perspective was conducted collaboratively by ONERA and JAXA. The validation of the numerical sonic boom prediction methodologies implemented at JAXA and ONERA has first been conducted using the experimental results of the D-SEND#1 drop test. This validation exercise showed an excellent code-to-code comparison and a good prediction of the experimentally measured sonic booms. These sonic boom prediction tools were then used in a numerical optimization process to improve the low boom characteristics of a initial glider aircraft configuration. Regarding the engine integration, the side-body engine out of three engine layouts (i.e., over-wing, under-wing, and side-body engines) showed the best compromise between low-boom and low-drag by utilizing the nacelle shock wave. The engine integration has large impact on the sonic boom loudness especially at the aft boom showing a single shock wave, even when the engine is mounted on side-body. The equivalent area distribution revealed the importance of the shock wave generated at the horizontal tail in reducing the aft boom loudness. Thus, the profile of horizontal tail was optimized to meet the target equivalent area distribution that was determined to realize double shock waves at the aft boom. The low-

boom design tool with consideration of the change of lift distribution successfully fragmented the aft boom into double shock waves by strengthening the leading edge shock wave at horizontal tail. The optimized shape realizes almost the same sonic boom loudness as the reference glider, which indicates the effectiveness of the low-boom design tool.

REFERENCES

[1] P. Coen, Supersonics Project Overview, Fundamental Aeronautics Program Technical Conference 2012.

[2] A. Murakami, Research Activities on Supersonic Technology at JAXA, The 2010 Asia-Pacific International Symposium on Aerospace Technology, 2010.

[3] A. Minelli, I. Salah el Din, G. Carrier, A. Zerbinati, J-A. Desideri, Cooperation and Competition Strategies in Multi-objective Shape Optimization - Application to Low-boom/Low-drag Supersonic Business Jet, 31st AIAA Applied Aerodynamics Conference, AIAA 2013-2678, 2013.

[4] Andrea Minelli. Aero-acoustic Shape Optimization of a Supersonic Business Jet. PhD Thesis, Analysis of PDEs [math.AP]. Université Nice Sophia Antipolis, 2013. HAL Id: tel-00938396, https://tel.archives-ouvertes.fr/tel-00938396v2, Submitted on 19 Feb 2014

[5] Y. Makino, K. Suzuki, M. Noguchi, and K. Yoshida, Nonaxisymmetrical Fuselage Shape Modification for Drag Reduction of Low-Sonic-Boom Airplane, AIAA Journal, Vol. 41, No. 8, 2003.

[6] M. Honda, K. Yoshida, D-SEND Project for Low Sonic Boom Design Technology, 28th Congress of the International Council of the Aeronautical Sciences, 2012.

[7] Plotkin, K. J., and Maglieri, D. J., Sonic Boom Research: History and Future, AIAA Paper 2003-3575, 2003.

[8] L. Cambier and M. Gazaix, elsA: An Efficient Object-Oriented Solution to CFD Complexity, AIAA 2002-0108, Reno, January 14-17, 2002.

[9] A. Refloch, B. Courbet, A. Murrone, P. Villedieu, C. Laurent, P. Gilbank, J. Troyes, L. Tessé, G. Chaineray, J.B. Dargaud, E. Quémerais, F. Vuillot, The CEDRE Software, AerospaceLab Journal, AL02-1, Issue 2 - March 2011 (http://www.aerospacelab-journal.org/sites/www.aerospacelab-journal.org/files/AL2-11.pdf)

[10] Adrien Loseille and Frédéric Alauzet. Continuous mesh framework, Part I: well-posed continuous interpolation error. SIAM Journal on Numerical Analysis, 49(1):38{60, 2011}

[11] K. Plotkin, J. Page, Extrapolation of sonic boom signatures from CFD solution, AIAA 2002-0922.

[12] I. Salah el Din, Contribution à l'optimisation de la forme aérodynamique d'un avion de transport supersonique en vue de la réduction du bang, Thèse de doctorat, Université de Poitiers, Décembre 2004.

[13] A.D. Taylor ; *The TRAPS sonic boom program* ; NOAA Technical memorandum ERL-ARL-87, July 1980 ;

[14] JAXA D-SEND#1 : http://www.aero.jaxa.jp/eng/research/frontier/sst/d-send.html

[15] A. Ueno, Y. Watanabe, Propulsion/airframe Integration Considering Low Drag and Low Sonic Boom, 29th Congress of the International Council of the Aeronautical Sciences, 2014.

[16] A. Ueno, Y. Watanabe, Multidisciplinary Design Optimization of Engine Layout for Supersonic Airliner. Koku-Uchu-Gijyutsu (Aerospace Technology Japan, the Japan Society for Aeronautical and Space Sciences), Vol. 14, 2015. (in Japanese)